

Continuum Field Description of Crack Propagation

I. S. Aranson, V. A. Kalatsky, and V. M. Vinokur

Argonne National Laboratory, 9700 South Cass Avenue, Argonne, Illinois 60439

(Received 9 December 1999)

We develop continuum field model for crack propagation in brittle amorphous solids. The model is represented by equations for elastic displacements combined with the order parameter equation which accounts for the dynamics of defects. This model captures all important phenomenology of crack propagation: crack initiation, propagation, dynamic fracture instability, sound emission, crack branching, and fragmentation.

PACS numbers: 62.20.Mk, 02.70.Bf, 46.50.+a

The dynamics of cracks is the long-standing challenge in solid state physics and materials science [1,2]. The phenomenology of the crack propagation is well established by recent experimental studies [3–9]: once a flux of energy to the crack tip passes the critical value, the crack becomes unstable and begins to branch and emit sound. Although this rich phenomenology is consistent with the continuum theory, it *fails to describe it* because the way the macroscopic objects break depends on the details of cohesion on microscopic scales [10].

Significant progress in understanding fracture dynamics was made by large-scale (about 10^7 atoms) molecular dynamics (MD) simulations [11,12]. Although limited to submicron samples, these simulations were able to reproduce several key features of the crack propagation, in particular, the initial acceleration of cracks and the onset of the dynamic instability. However, detailed understanding of the complex physics of the crack propagation still remains a challenge [13].

A uniform motion of the crack is relatively well understood in the framework of the continuum theory [14]. Most of the studies treat cracks as a front or interface separating broken and unbroken materials and propagating under the forces arising from elastic stresses in the bulk of material and additional cohesive stresses near the crack tip [15–18]. Although these investigations revealed some features of the oscillatory crack tip instability, they are based on built-in assumptions, e.g., on the specific dependence of the fracture toughness on velocity, structure of the cohesive stress, etc. To date there is no continuum model capable to describe in the same unified framework the whole phenomenology of the fractures, ranging from crack initiation to oscillations and branching.

In this Letter we present a continuum field theory of the crack propagation. Our model is the wave equations for the elastic deformations combined with the equation for the order parameter. The model captures all important phenomenology: crack initiation by small perturbation, quasistationary propagation, instability of fast cracks, sound emission, branching, and fragmentation.

Our model is a set of the elastodynamic equations coupled to the equation for the order parameter ρ , which

is related to the relative concentration of point defects in the amorphous material (e.g., microvoids) and characterizes *local order* [19]. We define $\rho = 1$ outside the crack (no defects) and $\rho = 0$ inside the crack (all the atomic bonds are broken). At the crack surface ρ varies from 0 to 1 on the scale much larger than the interatomic distance, justifying the continuum description of the crack [20]. Material fails to support tensile stress and breaks when ρ becomes below critical value ρ_c .

We consider the two-dimensional geometry focusing on the so-called type-I crack mode; see Fig. 1. Equations of motion for an elastic medium [21] are

$$\rho_0 \ddot{u}_i = \eta \Delta \dot{u}_i + \frac{\partial \sigma_{ij}}{\partial x_j}, \quad j = 1, 2. \quad (1)$$

u_i are the components of displacements, $\eta \Delta \dot{u}_i$ accounts for viscous damping, η is the viscosity coefficient [22], and ρ_0 is the density of material. In the following we set $\rho_0 = 1$. The stress tensor σ_{ij} is related to deformations via

$$\sigma_{ij} = \frac{E}{1 + \sigma} \left(u_{ij} + \frac{\sigma}{1 - \sigma} u_{ll} \delta_{ij} \right) + \nu \dot{\rho} \delta_{ij}, \quad (2)$$

where u_{ij} is the elastic strain tensor, E is the Young's modulus, and σ is the Poisson's ratio. To take into account the effect of weakening of material with the decrease of ρ we assume dependence of E upon ρ , $E = E_0 \rho$, where E_0 is the regular Young's modulus. The term $\sim \nu \dot{\rho}$ in Eq. (2) accounts for the hydrostatic pressure created due to generation of new defects; ν is the constant [23].

One can observe that Eqs. (1) are linear elasticity equations for $\rho = 1$, i.e., outside the crack, and have trivial dynamics for $\rho = 0$ (there is no dynamics inside crack).

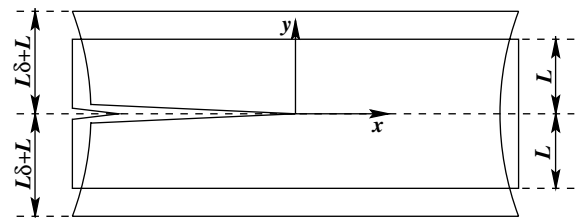


FIG. 1. Schematic representation of fixed-grips loading.

We assume that the order parameter ρ is governed by pure dissipative dynamics which can be derived from the “free-energy” type functional \mathcal{F} , i.e., $\dot{\rho} = -\delta\mathcal{F}/\delta\rho$. Following Landau ideas on phase transitions [24], we adapt the simplest form for the free energy $\mathcal{F} \sim \int dx dy [D|\nabla\rho|^2 + \phi(\rho)]$, where the “local potential energy” ϕ has minima at $\rho = 0$ and $\rho = 1$. Choosing the polynomial form for $\phi(\rho)$ we arrive at

$$\dot{\rho} = D\Delta\rho - a\rho(1 - \rho)F(\rho, u_{ll}) + f(\rho) \frac{\partial\rho}{\partial x_i} \dot{u}_i. \quad (3)$$

Coupling to the displacement field enters through the position of the unstable fixed point defined by the function $F(\rho, u_{ll})$, where u_{ll} is the trace of the strain tensor. The constraint imposed on $F(\rho, u_{ll})$ is that it must have one zero in interval $1 > \rho > 0$: $F(\rho_c, u_{ll}) = 0$, $1 > \rho_c > 0$, and $\partial_\rho F(\rho = \rho_c, u_{ll}) < 0$. The simplest form of F satisfying this constraint is $F(\rho, u_{ll}) = 1 - (b - \mu u_{ll})\rho$. Here b and μ are material constants related to such properties as crack toughness and strain to failure. D and a can be set to 1 by rescaling $t \rightarrow at$, $x_i \rightarrow \nu x_i$, where $\nu^2 = D/a$.

The last term in Eq. (3) represents the coupling of the order parameter to the velocity \dot{u} and is responsible for the localized shrinkage of the crack due to material motion. We find that the specific form of the function $f(\rho)$ is irrelevant, and take $f(\rho) = c\rho(1 - \rho)$ to ensure that f vanishes at $\rho = 0$ and $\rho = 1$, c being a dimensionless material constant. We have found that this term in Eq. (3) is crucial to maintain the sharp form of the crack tip.

Static solutions.—Equations (1)–(3) have a diplike solution corresponding to the open gap far behind the crack tip [a “groove” along the x axis for our geometry (see Fig. 1)]. The static one-dimensional equations read

$$\frac{\partial\rho u_{yy}}{\partial y} = 0, \quad (4)$$

$$\frac{\partial^2\rho}{\partial y^2} - \rho(1 - \rho)[1 - (b - \mu u_{yy})\rho] = 0,$$

with the fixed-grips boundary conditions (BC): $u_y(y = \pm L) = \pm L\delta$ (δ , the relative displacement), $\rho(y = \pm L) = 1$, and $\partial_y\rho(y = 0) = 0$. Exclusion of u_{yy} from Eqs. (4) yields

$$u_{yy} = C/\rho, \quad \partial_\xi^2\rho = \rho(1 - \rho)(1 - \beta\rho), \quad (5)$$

where C is a constant of integration [$C \int_0^L dy/\rho(y) = L\delta$], $\beta = b/(1 + \mu C)$, and $\xi = y\sqrt{1 + \mu C}$. The solution to Eq. (4) satisfying the BC for $L \rightarrow \infty$ is

$$\rho = \frac{\sqrt{(\beta + 1)(1 - \beta/2)} \cosh(\xi\sqrt{\beta - 1}) + 2 - \beta}{\sqrt{(\beta + 1)(1 - \beta/2)} \cosh(\xi\sqrt{\beta - 1}) + 2\beta - 1}. \quad (6)$$

This solution exists for $1 < \beta < 2$. A deep and wide crack opening is attainable if $2 - \beta = \epsilon \ll 1$. In this case the BC for u_y can be reduced to $\delta L = C[L + \pi\sqrt{3/(\epsilon b)}]$ yielding an equation for ϵ since $C = (b/2 - 1)/\mu$. For $\epsilon \ll 1$ the width of the crack opening d ,

defined as $\rho(d/2) = 1/2$, is $d = \sqrt{2/b} \ln(24/\epsilon)$. After exclusion of ϵ one arrives at

$$d = \sqrt{\frac{8}{b}} \ln \left[\frac{\sqrt{8b}}{\pi} L \left(\frac{2\mu\delta}{b-2} - 1 \right) \right]. \quad (7)$$

The solution to Eq. (7) exists only if δ exceeds some critical value δ_c given by $\delta_c \approx (b/2 - 1)/\mu$, which leads to the relation between the strain to failure δ_c and the material parameters μ and b . The logarithmic, instead of linear, dependence of crack opening on system size L in Eq. (7) is a shortcoming of the model resulting from an oversimplified dependence of the function F on u_{ll} .

To study the dynamics of cracks we perform numerical simulations of Eqs. (1)–(3). We use an explicit second-order scheme with the number of grid points up to 4000 \times 800. Selected results are presented in Figs. 2–5.

Some estimates of parameters of the model are in order. Our unit of length λ is the width of the craze zone

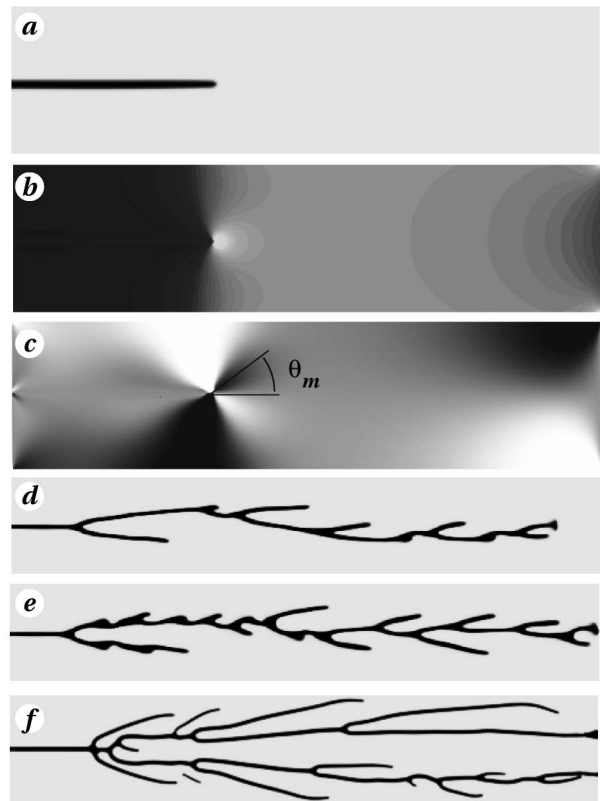


FIG. 2. (a) Grey-coded images of $\rho(x, y)$; (b) hydrostatic pressure $p = -(\sigma_{xx} + \sigma_{yy})$; (c) shear σ_{xy} . Domain size 800×200 , number of grid points 1600×400 , and $\delta = 0.05$, $\eta = 0.25$, $E_0 = 10$, $\sigma = 0.2$, $b = 2.25$, $c = 11$, $\nu = 2.3$, $\mu = 9.2$. (d) $\rho(x, y)$ for unstable propagation at $\delta = 0.089$ and (e) $\delta = 0.11$. Domain size 1200×200 , 2400×400 grid points. (f) $\rho(x, y)$ for propagation with fragmentation, $E_0 = 100$, $\sigma = 0.36$, $c = 16$, $\nu = 2.3$, $\mu = 54$, and $\delta = 0.03$, domain size 2000×400 , 4000×800 grid points. We displaced the initial crack (notch) from the center line by a small amount in the y direction to avoid degeneracy of the initial conditions.

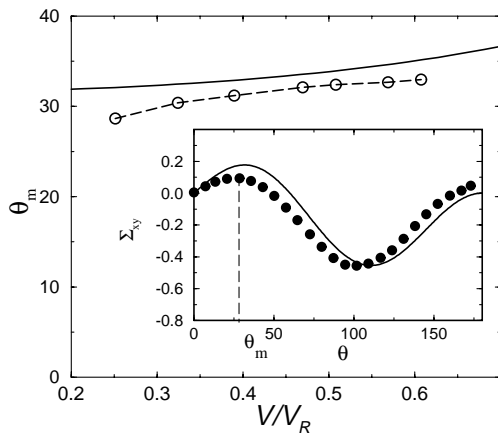


FIG. 3. θ_m vs crack velocity V for parameters of Figs. 2a–2c. Solid line shows θ_m vs V from linear elasticity [14]; \circ show result of numerical simulations. Inset: angular dependence of shear stress Σ_{xy} (filled circles). The dependence from linear elasticity theory for infinite crack is shown by solid line.

and is of the order of a micron in PMMA (Plexiglas) [20]. The unit of time τ is obtained from $\lambda \sim 1 \mu\text{m}$ and the Rayleigh wave speed $V_R \sim 10^3 \text{ m/s}$. Since in Eq. (1) $V_R \sim \sqrt{E_0}$, one obtains $\tau \sim \sqrt{E_0} \times 10^{-9} \text{ s}$. For the value of E_0 we used $E_0 = 10\text{--}100$. We will show later that it is consistent with the experimental data for PMMA. The Poisson's ratio σ for PMMA is 0.36. Simulations with $\sigma = 0.2$ (glass) did not show qualitative difference. The viscosity coefficient η can be extracted from the sound absorption data. For PMMA we find $\eta \approx 13/\sqrt{E_0}$.

Quasistationary propagation.—We consider crack propagation initiated from a long notch with the length of the order 100 units. At relatively small loadings δ we observe a quasistationary propagation (no oscillations).

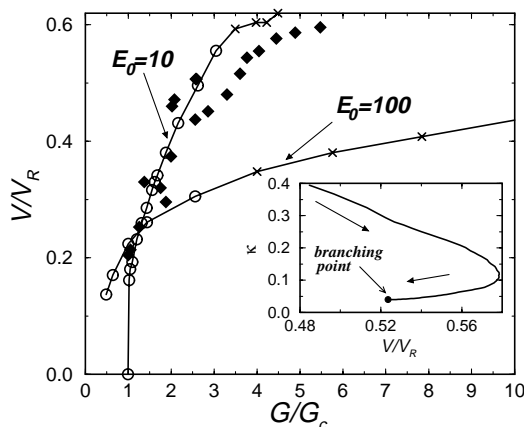


FIG. 4. Crack velocity V/V_R vs G/G_c , G_c corresponds to $V \approx 0.2V_R$. Open circles, \circ , correspond to stable propagation, crosses, \times , to unstable propagation, parameters are the same as for Fig. 2, and diamonds show the experimental data from Ref. [5] normalized by V_R in PMMA 926 m/s. Inset: curvature κ vs V/V_R for unstable crack at the level $\rho = 0.5$, parameters of Fig. 2f. Arrows indicate the progression of time.

The crack produces the stress concentration near the tip, while the stress is relaxed behind the tip; see Fig. 2b. The distribution of shear (Figs. 2c and 3) is close to that expected from the elasticity theory. The angular dependence $\Sigma_{xy}(\theta)$ of the shear stress σ_{xy} near the tip is close to the theoretical dependence $\sigma_{xy}(r, \theta) \sim r^{-1/2} \Sigma_{xy}^0 + \dots$, where $\Sigma_{xy}^0(\theta) = \sin(\theta) \cos(3\theta/2)$ obtained for the infinite stationary crack. The discrepancy can be attributed to finite-size effects and velocity correction. We computed the angle θ_m of the maximum shear stress vs crack speed V normalized by the Rayleigh wave speed V_R . (See Figs. 2c and 3.) As one derives from the linear elasticity, the angle increases with the speed of the crack [14], in agreement with our numerical results.

The calculated dependence of the crack tip velocity V on the effective fracture energy $G \sim \delta^2$, shown in Fig. 4, demonstrates a reasonable agreement with the experimental data from Ref. [5] for $E_0 = 10$. Similar dependence for $E_0 = 100$ lies significantly below the experimental curve. Thus, comparison with the experiment can be used to extract the value of parameter E_0 .

The instability of the crack occurs when the velocity becomes of the order of 55% of the Rayleigh speed for the parameters of Figs. 2a–2e. For parameters of Fig. 2f we have found a lower value of the critical velocity, namely about 32% of the Rayleigh speed. In all cases the instability manifests itself as pronounced velocity oscillations, crack branching and the sound emission from the crack tip. Figure 4, inset, shows dynamic crack tip blunting (decrease of crack tip curvature κ) as the velocity increases, similar to Ref. [25]. We find that for unstable cracks the curvature is a nonunique function of velocity.

Our calculations indicate the absence of the minimal crack velocity, the so-called velocity gap [10]. The initial velocity jump, seen experimentally as well as in some of our simulations (see Fig. 4), is attributed to the fact that the initial crack (notch) is too short or too blunt.

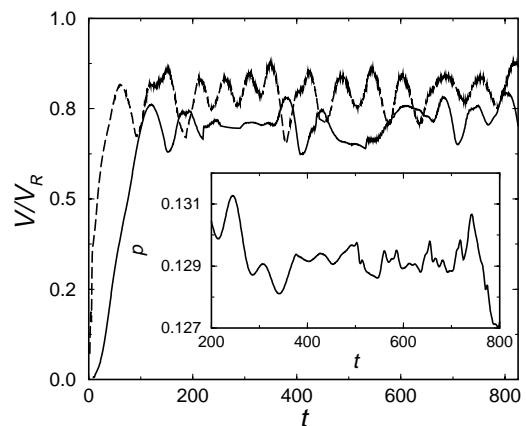


FIG. 5. The crack tip velocity V normalized by Rayleigh velocity V_R vs time for $\delta = 0.089$ (solid line) and $\delta = 0.11$ (dashed line), parameters of Figs. 2d and 2e. Inset: oscillations of pressure p far away from the crack tip for $\delta = 0.089$.

Instability of crack propagation.—Taking sufficiently large values of ν and c and starting from short cracks with the large load we observe consecutive crack branching. Since Eqs. (1)–(3) are homogeneous, these secondary crack branches typically retract after the stress at the tip of the shorter crack relaxes. Although this retracting may indeed take place, e.g., in vacuum the small cracks may heal; the oxidation of the crack surface and lattice trapping would prevent cracks from healing. In order to model these effects, one can introduce an additional field representing a concentration of oxygen and then couple it to the order parameter. In some simulations, we multiplied the right-hand side of Eq. (3) by a monotonic function $w(x - x_{\text{tip}})$: $w(x > 0) = 1$ and $w(x \rightarrow -\infty) \rightarrow 0$, where x_{tip} is the crack tip position. Thus, we slowed down the evolution of ρ behind the crack tip, which, in turn, prevents secondary cracks from healing. We succeeded in obtaining realistic crack forms; see Figs. 2d and 2e. For fast cracks “freezing” is not a necessity, since the retraction is rather slow. Figure 2f shows results without freezing: massive crack branching along with crack healing are present.

Far away from the crack tip we have registered oscillations of hydrostatic pressure (see Fig. 5, inset), which is a clear indication of the sound emission by the crack tip. The sound waves reflected from boundaries may also induce velocity oscillations, but they do not provide a mechanism for branching [26]. An increase in the applied displacement δ results in an increase of amplitude and the number of subbranches (compare Figs. 2d–2f and 5).

The value of E_0 which sets our time scale can be verified from the comparison with experiments for the frequency of oscillations. In experiments [4–8] the frequency is of the order 1 MHz, which results in the characteristic time of velocity oscillations $\tau_0 \sim 1 \mu\text{s}$. Our model gives $\tau_0 \sim 10^2 \tau \sim 0.1\text{--}1 \mu\text{s}$ for $E_0 = 10\text{--}100$.

We have developed a continuum field theory of the crack propagation. The central element of our approach is the order parameter description. It enables us to avoid the stress singularity at the crack tip and to derive the tip instability. Our model is complementary to MD simulations of cracks and allows for a description of fracture phenomena on large scales. The parameters of our model can be obtained from comparison with the experiment. It will be challenging to derive the order parameter equation from discrete models of crack propagation [27,28].

We are grateful to M. Marder, H. Swinney, J. Fineberg, V. Steinberg, H. Levine, E. Bouchaud, A. Bishop, and I. Daruka for stimulating discussions. This research is supported by U.S. DOE, Grant No. W-31-109-ENG-38.

[1] M. Marder and J. Fineberg, *Phys. Today* **49**, No. 9, 24 (1996).

[2] B. Lawn, *Fracture in Brittle Solids* (Cambridge University Press, Cambridge, 1993), 2nd ed.

- [3] J. A. Hauch, D. Holland, M. P. Marder, and H. L. Swinney, *Phys. Rev. Lett.* **82**, 3823 (1999).
- [4] E. Sharon and J. Fineberg, *Nature (London)* **397**, 333 (1999).
- [5] E. Sharon, S. P. Gross, and J. Fineberg, *Phys. Rev. Lett.* **74**, 5096 (1995); **76**, 2117 (1996).
- [6] J. F. Boudet, S. Ciliberto, and V. Steinberg, *Europhys. Lett.* **30**, 337 (1995).
- [7] J. F. Boudet, S. Ciliberto, and V. Steinberg, *J. Phys. II (France)* **6**, 1493 (1996).
- [8] J. Fineberg, S. Gross, M. P. Marder, and H. L. Swinney, *Phys. Rev. Lett.* **67**, 457 (1991).
- [9] P. Daguier, S. Henaux, E. Bouchaud, and F. Creuzet, *Phys. Rev. E* **53**, 5637 (1996).
- [10] J. Fineberg and M. Marder, *Phys. Rep.* **313**, 1 (1999).
- [11] F. Abraham, *Phys. Rev. Lett.* **77**, 869 (1996); S. J. Zhou, D. M. Beazley, P. S. Lomdahl, and B. L. Holian, *Phys. Rev. Lett.* **78**, 479 (1997); R. K. Kalia, A. Nakano, K. Tsuruta, and P. Vashishta, *Phys. Rev. Lett.* **78**, 689 (1997); D. Holland and M. Marder, *Phys. Rev. Lett.* **80**, 746 (1998); F. Cleri, S. Yip, D. Wolf, and S. R. Phillpot, *Phys. Rev. Lett.* **79**, 1309 (1997).
- [12] Special issue on dynamic fracture analysis [*Comput. Sci. Eng.* **1** (1999)].
- [13] Special issue on Defects in Materials: More Than Just a Clean Break [*Science* **281**, 943 (1998)].
- [14] L. B. Freund, *Dynamic Fracture Mechanics* (Cambridge University Press, New York, 1990).
- [15] E. A. Brener and V. I. Marchenko, *Phys. Rev. Lett.* **81**, 5141 (1998).
- [16] M. Adda-Bedia and M. Ben Amar, *Phys. Rev. Lett.* **76**, 1497 (1996); M. Adda-Bedia, R. Arias, M. Ben Amar, and F. Lund, *Phys. Rev. Lett.* **82**, 2314 (1999).
- [17] E. S. C. Ching, J. S. Langer, and H. Nakanishi, *Phys. Rev. E* **53**, 2864 (1996).
- [18] S. Ramanathan and D. S. Fisher, *Phys. Rev. Lett.* **79**, 877 (1997).
- [19] M. L. Falk and J. S. Langer, *Phys. Rev. E* **57**, 7192 (1998).
- [20] The characteristic scale of ρ is related to the damage zone width on the crack surface and is of the order of a micron for brittle polymers [the craze layer width, R. P. Kambour, *J. Polym. Sci. A-2* **4**, 17 (1966)].
- [21] L. D. Landau and E. M. Lifshitz, *Theory of Elasticity* (Pergamon Press, Oxford, 1964).
- [22] We assume incompressibility condition ($\text{div} \mathbf{v} = 0$).
- [23] The term $\nu \rho_t$ cannot be interpreted as the hydrostatic pressure due to thermal expansion. Although the temperature at the crack tip can be of the order of several hundred degrees, the thermal equilibrium is unlikely to be achieved at the crack tip; see, e.g., K. N. G. Fuller, P. G. Fox, and J. E. Field, *Proc. R. Soc. London A* **341**, 537 (1975); J. A. Kallivayalil and A. T. Zender, *Int. J. Fract.* **66**, 99 (1994).
- [24] L. D. Landau and E. M. Lifshitz, *Statistical Physics* (Pergamon Press, Oxford, 1980).
- [25] J. S. Langer, *Phys. Rev. E* (to be published).
- [26] The interaction with sound can be reduced by introducing additional damping term $\sim \dot{\mathbf{u}}$ to the right-hand side of Eq. (1).
- [27] M. Marder, *Phys. Rev. E* **54**, 3442 (1996).
- [28] D. A. Kessler and H. Levine, *Phys. Rev. E* **59**, 5154 (1999).